

February 17, 1998

Cosmology in the Next Millennium: Combining MAP and SDSS Data to Constrain Inflationary Models

Yun Wang, David N. Spergel, & Michael A. Strauss^{1,2}

Princeton University Observatory

Peyton Hall, Princeton, NJ 08544

email: ywang,dns,strauss@astro.princeton.edu

Abstract

The existence of primordial adiabatic Gaussian random-phase density fluctuations is a generic prediction of inflation. The properties of these fluctuations are completely specified by their power spectrum $A_S^2(k)$. The basic cosmological parameters and the primordial power spectrum together completely specify predictions for the cosmic microwave background radiation anisotropy and large scale structure. Here we show how we can strongly constrain both $A_S^2(k)$ and the cosmological parameters by combining the data from the Microwave Anisotropy Probe (MAP) and the galaxy redshift survey from the Sloan Digital Sky Survey (SDSS). We allow $A_S^2(k)$ to be a free function, and thus probe features in the primordial power spectrum on all scales. If we assume that the cosmological parameters are known *a priori*, the primordial power spectrum in 20 steps in $\log k$ to $k \leq 0.5h\text{Mpc}^{-1}$ can be determined to $\sim 10\%$ accuracy for $k \sim 0.01h\text{Mpc}^{-1}$, and to $\sim 1\%$ accuracy for $k \sim 0.1h\text{Mpc}^{-1}$. The uncertainty in the primordial power spectrum increases by less than a factor of 2 if we solve simultaneously for the dimensionless Hubble constant h , the cosmological constant Λ , the baryon fraction Ω_b , the reionization optical depth τ_{ri} , and the effective bias between the matter density field and the galaxy redshift density field b_{eff} . Alternately, if we restrict $A_S^2(k)$ to be a power law, we find that inclusion of the SDSS data breaks the degeneracy between the amplitude of the power spectrum and the optical depth inherent in the MAP data, reduces the uncertainties in the determination of the matter density and the cosmological constant, and allows a determination of the galaxy bias parameter. Thus, combining the MAP and SDSS data allows the independent measurement of important cosmological parameters, and a model-independent

¹Alfred P. Sloan Foundation Fellow

²Cottrell Scholar of Research Corporation

measurement of the primordial power spectrum, giving us valuable information on physics in the early Universe, and providing clues to the correct inflationary model.

1. Introduction

Standard cosmological models require ad-hoc initial conditions to solve three basic conundrums: why the universe is homogeneous on large scales, why the cosmological density parameter Ω_m is close to unity, and why the large-scale distribution of matter has the amplitude it does. Inflation provides compelling solutions to all these problems (Kolb & Turner 1990).

The cosmic microwave background radiation (CMB) is observed to be isotropic to an accuracy of better than 10^{-4} . This implies that the Universe was homogeneous to this accuracy over many horizon scales at last scattering. Within the standard cosmology there is no causal process which could have created the observed homogeneity. The basic idea of inflation is that the observable Universe grew from an initial patch small enough to fit inside the horizon. It is hypothesized that there were particle physics mechanisms which led to the rapid expansion of the early Universe required to produce the huge growth factor necessary to solve the cosmological problems above. In this paper, we assume that inflation produces primordial adiabatic Gaussian random-phase density fluctuations due to quantum fluctuations in the inflaton field. The properties of these fluctuations are completely specified by their power spectrum $A_S^2(k)$ ³.

There currently exists a broad range of inflationary models (Kolb 1996, Turner 1997). Some of these models predict power spectra that are almost exactly scale-invariant (Linde 1983), or are described by a power law with spectral index less than one (Freese, Frieman, & Olinto 1990, La & Steinhardt 1991), while others predict power spectra with slowly varying spectral indices (Wang 1994), or with broken scale invariance (Holman et al. 1991ab, Adams, Ross, & Sarkar 1997, Lesgourgues, Polarski, & Starobinsky 1997).

Indeed, there are physical reasons to believe that the primordial power spectrum has breaks in its power-law form. In effective (i.e., not complete) theories with two scalar fields, inflation may occur in two stages. The two stages of inflation can generate density perturbations with different power-law indices, with a step in amplitude of the primordial power spectrum on the scale of the transition between the two phases (Holman et al. 1991ab). Fry & Wang (1992) found that such models can have a significant signature on small-scale CMB anisotropies.

Recently, Adams, Ross, & Sarkar (1997) proposed a new multiple inflation model. Since attempts at an unified description of the strong, weak and electromagnetic interactions

³Certain two-field inflationary models predict isocurvature as well as adiabatic fluctuations (Kofman & Linde 1987). Since the CMB and LSS predictions of isocurvature models differ significantly from adiabatic models and since these differences are not degenerate with parameter variation, we could, in principle, also fit for an isocurvature power spectrum. However, in this paper, we limit ourselves to considering adiabatic fluctuations.

usually involve several stages of spontaneous symmetry breaking, they considered the effects of such symmetry breaking during an era of inflation in supergravity models. They found that there can be a succession of short bursts of inflation; the density perturbations produced during each burst is nearly scale-invariant but with differing amplitudes, and between each burst there is a brief period during which scale-invariance is badly broken.

Given the range of possibilities for the primordial power spectrum, we would like to quantify how well it can be measured generically. Thus, we take the primordial power spectrum to be a free function in this paper.

The upcoming data from the Microwave Anisotropy Probe (MAP; cf., Bennett et al. 1997; <http://map.gsfc.nasa.gov>) and the Sloan Digital Sky Survey (SDSS; cf., Gunn & Weinberg 1996) provide a unique opportunity for constraining inflationary models. It is customary to expand the temperature fluctuations in the CMB into spherical harmonics: $\delta T/T(\hat{\mathbf{r}}) = \sum_{l,m} a_{T,lm} Y_{lm}(\hat{\mathbf{r}})$, where $\hat{\mathbf{r}}$ is the unit direction vector in the sky. MAP measures the angular power spectrum (Seljak & Zaldarriaga 1996)

$$C_{Tl} \equiv \langle |a_{T,lm}|^2 \rangle = (4\pi)^2 \int \frac{dk}{k} A_S^2(k) |\Delta_{Tl}(k, \tau = \tau_0)|^2, \quad (1)$$

where $A_S^2(k)$ is the power spectrum of the primordial density fluctuations (defined such that $A_S^2(k) = 1$ for the scale-invariant Harrison-Zel'dovich spectrum), $\Delta_{Tl}(k, \tau = \tau_0)$ is an integral over conformal time τ of the sources which generate the CMB fluctuations, and τ_0 is the conformal time today.

The power spectrum of mass fluctuations in the linear regime today is

$$P(k) = P_0 k A_S^2(k) T^2(k), \quad (2)$$

where P_0 is a normalization constant, and $T(k)$ is the transfer function, which depends on physics at matter-radiation equality and decoupling.

The galaxy redshift survey from the SDSS (cf., Strauss 1997 for a description) will allow a determination of $P_G(k)$, the galaxy power spectrum in redshift space. The quantity $P_G(k)$ differs from the mass power spectrum $P(k)$ due to two effects. First, the galaxy distribution may be biased with respect to the mass distribution. On large scales, models (Weinberg 1995; Kauffmann, Nusser, & Steinmetz 1997; Scherrer & Weinberg 1997) indicate that the mass and galaxy density fields are directly proportional to one another. The proportionality constant is referred to as the galaxy bias parameter, b . In addition, peculiar velocities cause the density contrast of galaxies in redshift space to appear appreciably stronger than in real space. In linear theory, the power spectrum is boosted by a factor $1 + \frac{2}{3}\beta + \frac{1}{5}\beta^2$, where $\beta \equiv \Omega_m^{0.6}/b$ (Ω_m is the matter density in units of the critical density of the Universe $\rho_c \equiv 3H_0^2/(8\pi G)$, with H_0 denoting the Hubble constant). The net result (Kaiser 1987; cf., Hamilton 1997 for a review) is that on linear scales, the galaxy power spectrum is given by:

$$P_G(k) = b^2 \left(1 + \frac{2}{3}\beta + \frac{1}{5}\beta^2 \right) P(k) \equiv b_{\text{eff}}^2 P(k). \quad (3)$$

The observables C_{Tl} and $P_G(k)$ depend on the cosmological parameters H_0 , Ω_b (baryon density in units of ρ_c), Ω_m , Ω_Λ (density contribution from the Cosmological Constant in units of ρ_c), and τ_{ri} (reionization optical depth) only through $\Delta_{Tl}(k, \tau = \tau_0)$, b_{eff} , and $T(k)$. The MAP data alone will allow rather tight constraints on the baryon/photon ratio (which determines $\Omega_b h^2$), the matter/photon ratio (which determines $\Omega_m h^2$), and the geometry of the universe, and test the basic inflationary scenario (Spergel 1994; Jungman et al. 1996; Bond, Efstathiou & Tegmark 1997; Zaldarriaga, Spergel & Seljak 1997; Dodelson, Kinney & Kolb 1997; Lidsey et al. 1997; Copeland, Grivell & Liddle 1997). However, there is a near-degeneracy in several sets of parameters (Bond et al. 1994; Bond, Efstathiou & Tegmark 1997; Zaldarriaga, Spergel & Seljak 1997; Huey & Dave 1997) including the overall amplitude of the power spectrum at $k \sim 0.1 h\text{Mpc}^{-1}$ and the optical depth. Since $\Delta_{Tl}(k, \tau = \tau_0)$ and $T(k)$ depend on the cosmological parameters differently, by combining the MAP and SDSS data, we can break these degeneracies and determine cosmological parameters to impressive accuracies. Two other recent papers have also considered how well cosmological parameters can be constrained with the combination of future CMB and galaxy survey data: Tegmark (1997) has studied a somewhat different and smaller set of the cosmological parameters than we consider here, and Hu, Eisenstein, & Tegmark (1997) have tested the sensitivity of the data to the neutrino mass, which we do not consider in this paper. See also Lineweaver & Barbosa (1998) and Webster et al. (1998) who fit for cosmological parameters using the best available CMB and redshift data available now.

Both C_{Tl} and $P_G(k)$ are proportional to the amplitude of the power spectrum of the primordial density fluctuations $A_S^2(k)$. Because of the finite resolution of the MAP satellite, the errors on the C_{Tl} increase rapidly with wavenumber for $l \gtrsim 800$, while the errors on $P_G(k)$ from the SDSS decrease with wavenumber; MAP and SDSS thus quite naturally complement each other in the determination of $A_S^2(k)$. Assuming that inflation occurred, all the obtainable information about the inflationary model is contained in $A_S^2(k)$.

Some inflationary models predict a significant gravity wave contribution to the microwave background fluctuation spectrum at small l . However, even in these models, gravity waves do not make a significant contribution to the microwave background fluctuation spectrum at $l \gtrsim 100$ (Crittenden et al. 1993, Dodelson, Knox, & Kolb 1994, Allen & Koranda 1995, Wang 1996, Turner & Wang 1996). Since most of the information on the cosmological parameters comes from relatively small angular scales ($l \gtrsim 100$), the inclusion of tensor perturbations would not change our results qualitatively.

We parameterize $A_S^2(k)$ by a series of steps equally spaced in $\log k$ bins, each step with a constant amplitude in its bin. By taking these amplitudes to be independent parameters, we probe features in the primordial power spectrum on all scales. The model-independent measurement of the primordial power spectrum from the combined MAP and SDSS data should shed light on our understanding of the early Universe.

In Section 2, we present the statistical technique we use in estimating errors of

parameters. We illustrate the accuracy in the determination of cosmological parameters in Section 3, where we take the primordial power spectrum to be a pure power law. In Section 4, we discuss the determination of the primordial power spectrum, using the stepwise parameterization described above. Section 5 contains a summary of the paper.

2. The Fisher Information Matrix

The Fisher information matrix of a given set of parameters, \mathbf{s} , approximately quantifies the amount of information on \mathbf{s} that we “expect” to get from our future data. The Fisher matrix can be written as

$$F_{ij} = -\frac{\partial^2 \ln L}{\partial s_i \partial s_j}, \quad (4)$$

where L is the likelihood function, the expected probability distribution of the observables given parameters \mathbf{s} . The Cramér-Rao inequality (Kendall & Stuart 1969) states that no unbiased method can measure the i -th parameter with standard deviation less than $1/\sqrt{F_{ii}}$ if other parameters are known, and less than $\sqrt{(\mathbf{F}^{-1})_{ii}}$ if other parameters are estimated from the data as well. Note that the derivatives in Equation (4) are calculated assuming that the cosmological parameters are given by an a priori model, and thus the errors on the parameters are somewhat dependent on the assumed model.

The likelihood function L in principle can be that of the raw data; see, for example, the discussion in Tegmark et al. (1998) and Dodelson, Hui, & Jaffe (1997). But as Tegmark, Taylor, & Heavens (1997) describe, it is far more convenient to work with the data in a more compressed form. For the galaxy data, we work with the observed galaxy power spectrum, which can be determined using the techniques reviewed, e.g., in Strauss (1997) or Tegmark et al. (1998). The values of the measured power spectrum are approximately statistically independent if measured at values of k spaced at intervals of $2\pi/R$, where R is the characteristic length of the survey volume. Similarly, for a full-sky CMB mapping experiment like MAP, the individual C_l ’s are statistically independent.

2.1. CMB Data

MAP will measure the CMB polarization as well as temperature anisotropy. The CMB radiation field is described by a 2×2 intensity tensor I_{ij} . The Stokes parameters are $Q \equiv (I_{11} - I_{22})/4$ and $U \equiv I_{12}/2$, while the temperature anisotropy is $\delta T/T \equiv (I_{11} + I_{22})/4$. The temperature anisotropy can be expanded in standard spherical harmonics, while $(Q \pm iU)$ have to be expanded using spin weight ± 2 spherical harmonics ${}_{\pm 2}Y_{lm}$ (Gelfand et al. 1963, Goldberg et al. 1967, Zaldarriaga & Seljak 1997; see also Kamionkowski, Kosowsky,

& Stebbins 1997 for an alternative expansion):

$$\begin{aligned}\delta T/T(\hat{\mathbf{n}}) &= \sum_{lm} a_{T,lm} Y_{lm}(\hat{\mathbf{n}}), \\ (Q + iU)(\hat{\mathbf{n}}) &= \sum_{lm} a_{2,lm} {}_2Y_{lm}(\hat{\mathbf{n}}), \\ (Q - iU)(\hat{\mathbf{n}}) &= \sum_{lm} a_{-2,lm} {}_{-2}Y_{lm}(\hat{\mathbf{n}}),\end{aligned}\quad (5)$$

where $\hat{\mathbf{n}}$ is the unit direction vector in the sky. The even and odd parity linear combinations of $a_{2,lm}$ and $a_{-2,lm}$ are

$$\begin{aligned}a_{E,lm} &= -(a_{2,lm} + a_{-2,lm})/2, \\ a_{B,lm} &= i(a_{2,lm} - a_{-2,lm})/2.\end{aligned}\quad (6)$$

Note that $a_{E,lm}$ and $a_{B,lm}$ behave analogously to the electric and magnetic fields respectively under parity transformation. The statistics of the CMB are specified by the power spectra of the variables ($a_{T,lm}$, $a_{E,lm}$, $a_{B,lm}$) together with their cross-correlations. For density (scalar) perturbations, the odd parity mode B vanishes. The power spectra can be written as (Seljak & Zaldarriaga 1996)

$$\begin{aligned}C_{Tl} &\equiv \langle |a_{T,lm}|^2 \rangle = (4\pi)^2 \int \frac{dk}{k} A_S^2(k) |\Delta_{Tl}(k, \tau = \tau_0)|^2, \\ C_{El} &\equiv \langle |a_{E,lm}|^2 \rangle = (4\pi)^2 \int \frac{dk}{k} A_S^2(k) |\Delta_{El}(k, \tau = \tau_0)|^2, \\ C_{Cl} &\equiv \langle a_{T,lm}^* a_{E,lm} \rangle = (4\pi)^2 \int \frac{dk}{k} A_S^2(k) \Delta_{Tl}(k, \tau = \tau_0) \Delta_{El}(k, \tau = \tau_0),\end{aligned}\quad (7)$$

where $\Delta_{T,El}(k, \tau = \tau_0)$ are integrals over conformal time τ of the sources which generate the CMB temperature fluctuations and polarization.

If we assume that the errors in the $C_{T,E,Cl}$ and the $P(k_q)$ are Gaussian-distributed, we can follow Jungman et al. (1996), Goldberg & Strauss (1998), Tegmark (1997), and Zaldarriaga, Spergel, & Seljak (1997) in writing the Fisher matrix for the combined MAP and SDSS data as:

$$F_{ij} = \sum_l \sum_{X,Y} \frac{\partial C_{Xl}}{\partial s_i} \text{Cov}^{-1}(C_{Xl}, C_{Yl}) \frac{\partial C_{Yl}}{\partial s_j} + \sum_q \frac{1}{\sigma_{P_q}^2} \frac{\partial P_G(k_q)}{\partial s_i} \frac{\partial P_G(k_q)}{\partial s_j}, \quad (8)$$

where $X, Y = T, E, C$. $\text{Cov}^{-1}(C_{Xl}, C_{Yl})$ is the inverse of the covariance matrix $\text{Cov}(C_{Xl}, C_{Yl}) = \langle \Delta C_{Xl} \Delta C_{Yl} \rangle$. For each l , one has to invert the covariance matrix and sum over X and Y . σ_{P_q} are the standard errors in the measurement of $P(k_q)$ (equation 12 below). We compute the C_{Xl} and $P(k)$ using the CMBFAST Boltzmann code by Uroš Seljak and Matias Zaldarriaga (Seljak & Zaldarriaga 1996). We calculate those derivatives

which cannot be found analytically by finite differences, with the step taken to be 5% of the value of each parameter.

The covariance matrix of CMB power spectrum estimators has diagonal elements given by (Seljak 1996, Zaldarriaga & Seljak 1997, Kamionkowski, Kosowsky, & Stebbins 1997):

$$\begin{aligned}\text{Cov}(C_{Tl}^2) &= \frac{2}{(2l+1)f_{sky}} \left(C_{Tl} + w_T^{-1} B_l^{-2} \right)^2, \\ \text{Cov}(C_{El}^2) &= \frac{2}{(2l+1)f_{sky}} \left(C_{El} + w_P^{-1} B_l^{-2} \right)^2, \\ \text{Cov}(C_{Cl}^2) &= \frac{1}{(2l+1)f_{sky}} \left[C_{Cl}^2 + \left(C_{Tl} + w_T^{-1} B_l^{-2} \right) \left(C_{El} + w_P^{-1} B_l^{-2} \right) \right],\end{aligned}\quad (9)$$

while the off-diagonal matrix elements are:

$$\begin{aligned}\text{Cov}(C_{Tl}C_{El}) &= \frac{2}{(2l+1)f_{sky}} C_{Cl}^2, \\ \text{Cov}(C_{Tl}C_{Cl}) &= \frac{2}{(2l+1)f_{sky}} C_{Cl} \left(C_{Tl} + w_T^{-1} B_l^{-2} \right), \\ \text{Cov}(C_{El}C_{Cl}) &= \frac{2}{(2l+1)f_{sky}} C_{Cl} \left(C_{El} + w_P^{-1} B_l^{-2} \right),\end{aligned}\quad (10)$$

where f_{sky} is the fraction of sky which is mapped. We have defined $w_{(T,P)}^{-1} \equiv \sigma_{(T,P)}^2 \theta_{fwhm,c}^2$, where $\sigma_{T,P}$ is the noise per pixel in the temperature and the polarization measurements, and θ_{fwhm} is the full width at half maximum of the beam in radians. The quantity $B_l^2 \equiv \exp \left[- (0.425 \theta_{fwhm} l)^2 \right]$ is the window function of the Gaussian beam.

For MAP, both temperature and polarization data are obtained from the same experiment by adding and differencing the two polarization states, hence $\sigma_T^2 = \sigma_P^2/2$, and the noise and polarization signals are uncorrelated. MAP's resolution at its three highest frequency channels (40, 60, and 90 GHz) is anticipated to be $\theta_{fwhm} = 0.47^\circ$, 0.35° , and 0.21° respectively, with the corresponding $\sigma_T = 27 \mu\text{K}$, $35 \mu\text{K}$, and $35 \mu\text{K}$ for its two year nominal mission (Bennett et al. 1997; <http://map.gsfc.nasa.gov>). We do a weighted average in the three channels c , yielding

$$\begin{aligned}w_T &= \sum_c w_T^c = \sum_c \frac{1}{\sigma_{T,c}^2 \theta_{fwhm,c}^2} = \frac{1}{(0.10 \mu\text{K})^2}, \\ w_P &= w_T/2, \\ B_l^2 &= \frac{\sum_c w_T^c B_{l,c}^2}{\sum_c w_T^c} = \frac{\sum_c e^{-l^2 \sigma_{b,c}^2} / \left(\sigma_{T,c}^2 \theta_{fwhm,c}^2 \right)}{\sum_c 1 / \left(\sigma_{T,c}^2 \theta_{fwhm,c}^2 \right)}.\end{aligned}\quad (11)$$

2.2. Galaxy Data

We take the SDSS standard error in the measured galaxy power spectrum from Feldman, Kaiser, & Peacock (1994). For the power spectrum determined over a volume in k -space of V_k :

$$\frac{\sigma_P}{P_G(k)} = \left(\frac{(2\pi)^3 \int d^3\mathbf{r} \bar{n}^4(\mathbf{r}) \psi^4(\mathbf{r}) \left[1 + \frac{1}{\bar{n}(\mathbf{r}) P_G(k)} \right]^2}{V_k \left[\int d^3\mathbf{r} \bar{n}^2(\mathbf{r}) \psi^2(\mathbf{r}) \right]^2} \right)^{1/2}, \quad (12)$$

where $\bar{n}(\mathbf{r})$ is the selection function, and $\psi(\mathbf{r})$ is the weighting function. For spherical shells, $V_{k_q} = \frac{4}{3}\pi(k_q^3 - k_{q-1}^3)$, where again, the spacing between the k_q is $2\pi/R$. We choose $R = 1466 h^{-1}$ Mpc for the SDSS, following Goldberg & Strauss (1998). We use the SDSS selection function calculated by Goldberg & Strauss (1998) using a mock SDSS redshift sample created by D. Weinberg (cf., Cole et al. 1998). We take the weighting function $\psi(\mathbf{r}) = 1$ throughout. Equation (12) assumes that the power estimates in each k band are uncorrelated. Goldberg & Strauss (1998) show that this assumption causes at most a 10% underestimation of the true errors of parameters.

3. Determination of the Cosmological Parameters

In this section, we assume a simple power-law model for the primordial power spectrum, $k A_S^2(k) \propto k^{n_S}$, and ask how well cosmological parameters can be determined by combining the MAP and SDSS data. We consider h , Ω_Λ , Ω_b , τ_{ri} , n_S , Ω_m , $C_2 \equiv |a_{T,2m}|^2$ (which sets the CMB normalization), and b_{eff} as free parameters.

The Fisher matrix depends on the true underlying power spectrum. We consider here five models, standard cold dark matter model (SCDM), the CDM model with cosmological constant (Λ CDM), open Λ CDM (O Λ CDM), and open CDM (OCDM). The model values of the cosmological parameters are shown in Table 1. The C_2 values in Table 1 are obtained by normalizing the models to the COBE four-year data, following Bunn & White (1997). We take the galaxy bias parameter to be $b = 1/\sigma_8$, with σ_8 derived using the model C_2 value. Note that as we vary parameters to compute the Fisher matrix, we keep $\Omega_m + \Omega_\Lambda = 1$ for the SCDM and Λ CDM models, because these models are flat by definition. To allow for the simultaneous determination of Ω_m and Ω_Λ , we consider a model close to Λ CDM, the open Λ CDM (O Λ CDM), to avoid comparing open models with flat models in the calculation of derivatives.

In the linear theory of mass density fluctuations, the bias factor b is degenerate with the CMB normalization C_2 . Nonlinear effects in the present-day galaxy power spectrum break this degeneracy. We include nonlinear effects following Peacock & Dodds (1996).

Table 1: Model values of cosmological parameters

	h	Ω_Λ	Ω_b	τ_{ri}	n_S	Ω_m	C_2	$b = 1/\sigma_8$
SCDM	0.5	0	0.05	0.05	1	1	1.139×10^{-10}	0.83
Λ CDM	0.65	0.7	0.06	0.1	1	0.3	1.455×10^{-10}	1.29
O Λ CDM	0.65	0.6	0.06	0.1	1	0.3	1.364×10^{-10}	1.42
OCDM	0.65	0	0.06	0.05	1	0.4	1.607×10^{-10}	1.72

Given a linear power spectrum $P_L(k_L)$, the effective local power law index can be defined as

$$n_{\text{eff}}(k_L) = n_L(k_L) = \left. \frac{d \ln P_L}{d \ln k} \right|_{k=k_L/2}. \quad (13)$$

The nonlinear power spectrum $P_{NL}(k)$ is related to the linear power spectrum by

$$\Delta_{NL}^2(k_{NL}) = f_{NL}(\Delta_L^2(k_L)), \quad (14)$$

where $\Delta_L^2(k_L) \equiv k_L^3 P_L(k_L)/(2\pi^2)$, and $\Delta_{NL}^2 \equiv k^3 P_{NL}(k)/(2\pi^2)$.

$$f_{NL}(x) = x \left[\frac{1 + B\gamma x + [Ax]^{\alpha\gamma}}{1 + ([Ax]^\alpha g^3(\Omega)/[Vx^{1/2}])^\gamma} \right]^{1/\gamma} \quad (15)$$

with

$$\begin{aligned} A &= 0.482 (1 + n_{\text{eff}}/3)^{-0.947}, \\ B &= 0.226 (1 + n_{\text{eff}}/3)^{-1.778}, \\ \alpha &= 3.310 (1 + n_{\text{eff}}/3)^{-0.244}, \\ \gamma &= 0.862 (1 + n_{\text{eff}}/3)^{-0.287}, \\ V &= 11.55 (1 + n_{\text{eff}}/3)^{-0.423}, \end{aligned} \quad (16)$$

and (Carroll, Press, & Turner 1992)

$$g(\Omega) = \frac{5}{2} \Omega_m \left[\Omega_m^{4/7} - \Omega_\Lambda + (1 + \Omega_m/2)(1 + \Omega_\Lambda/70) \right]^{-1}. \quad (17)$$

The nonlinear wavenumber is related to the linear wavenumber by

$$k_{NL} = k_L [1 + \Delta_{NL}^2(k_{NL})]^{1/3}. \quad (18)$$

Note that although our consideration of nonlinear effects is adequate in the context of this paper, it is inaccurate in several ways. First, even though we include nonlinear effects in $P(k)$, we still use Kaiser's linear relation for redshift effects. Proper consideration of

redshift distortion on small scales (Fisher & Nusser 1996, Hatton & Cole 1997) will lead to an effective bias b_{eff} which depends on k as well as the cosmological parameters b and Ω_m . Second, as the strength of the baryon-induced wiggles in the power spectrum is proportional to Ω_b/Ω_m , they are more pronounced in the Λ CDM and OCDM models. The Peacock & Dodds (1996) non-linear formulae only apply to *smooth* linear power spectra; we therefore smooth the linear power spectra (using the analytical formulae in Eisenstein & Hu 1997) before applying the non-linear formulae. Since we are discarding the information contained in the baryon-induced wiggles, we obtain overestimates of the true errors. Third, non-linear effects will cause the error distribution of the power spectrum estimation to become non-Gaussian, and will cause mode-mixing between estimates of the power spectrum we have assumed here to be independent (cf., Jain & Bertschinger 1994). These effects are difficult to include in the Fisher matrix formalism, and we do not attempt to do so here. We carry out all calculations in this section to two limits in the k_q of the galaxy power spectrum, $k_{\text{max}} = 0.1 h \text{ Mpc}^{-1}$ and $k_{\text{max}} = 0.5 h \text{ Mpc}^{-1}$. The Peacock & Dodds (1996) formalism indicates that for the models considered here, non-linear effects become significant for values of k somewhat larger than $0.1 h \text{ Mpc}^{-1}$. So the former value of k_{max} corresponds to a scale where non-linear effects are negligible, while the latter corresponds to a scale $2\pi/k \approx 12h^{-1}\text{Mpc}$ where nonlinear effects are becoming strong. It is work for the future to check the validity of our calculations in this non-linear regime.

To calculate the Fisher matrix, we need the derivatives of the C_{Xl} 's (X denotes T , E , C) and $P_G(k) = b_{\text{eff}}^2 P_{NL}(k)$ with respect to the cosmological parameters. The derivatives with respect to C_2 and b_{eff} can be found analytically:

$$\begin{aligned} \frac{\partial C_{Xl}}{\partial \ln C_2} &= C_{Xl}, \\ \frac{\partial C_{Xl}}{\partial \ln b_{\text{eff}}} &= 0, \\ \frac{\partial P_G(k)}{\partial \ln C_2} &= P_G(k) \frac{\partial \ln f_{NL}(x)}{\partial \ln x}, \\ \frac{\partial P_G(k)}{\partial \ln b_{\text{eff}}} &= 2 P_G, \end{aligned} \quad (19)$$

where $x \equiv \Delta_L^2(k_L)$, and k_L is related to k via equation (18). The derivatives with respect to the other cosmological parameters are calculated numerically by finite differences.

Tables 2, 3, 4, and 5 show the Fisher Matrix $1-\sigma$ error bars for the cosmological parameters, $\Delta s_i = \sqrt{(\mathbf{F}^{-1})_{ii}}$ for SCDM, Λ CDM, $\Omega\Lambda$ CDM, and OCDM respectively. For each parameter, we list the errors for six cases: the MAP temperature data taken alone, the MAP temperature data with SDSS data to $k_{\text{max}} = 0.1 h \text{ Mpc}^{-1}$, the MAP temperature data with SDSS data to $k_{\text{max}} = 0.5 h \text{ Mpc}^{-1}$, and the corresponding results when MAP polarization data are included as well.

The peak features (called “Doppler peaks”, “acoustic peaks”, or “Sakharov peaks”) in

Table 2: Fisher Matrix $1-\sigma$ error bars for the cosmological parameters of SCDM.

1- σ error	MAP ^T	MAP ^T + SDSS ¹	MAP ^T + SDSS ²	MAP ^(T+P)	MAP ^(T+P) + SDSS ¹	MAP ^(T+P) + SDSS ²
$\Delta \ln C_2$	0.14	9.20×10^{-2}	1.52×10^{-2}	5.42×10^{-2}	4.90×10^{-2}	1.51×10^{-2}
$\Delta \ln h$	3.39×10^{-2}	3.08×10^{-2}	2.05×10^{-2}	2.81×10^{-2}	2.59×10^{-2}	1.83×10^{-2}
$\Delta \Omega_\Lambda$	8.66×10^{-2}	7.80×10^{-2}	5.06×10^{-2}	7.05×10^{-2}	6.46×10^{-2}	4.40×10^{-2}
$\Delta \ln(\Omega_b h^2)$	2.15×10^{-2}	2.09×10^{-2}	1.87×10^{-2}	1.94×10^{-2}	1.89×10^{-2}	1.75×10^{-2}
$\Delta \ln \tau_{ri}$	1.71	1.21	0.40	0.39	0.38	0.28
$\Delta \ln n_S$	9.29×10^{-3}	8.36×10^{-3}	6.40×10^{-3}	6.20×10^{-3}	5.91×10^{-3}	4.97×10^{-3}
$\Delta \ln b_{eff}$		5.82×10^{-2}	2.83×10^{-2}		5.55×10^{-2}	2.31×10^{-2}

Note. — “T” denotes temperature only, “(T+P)” denotes temperature plus polarization for MAP data. “1” and “2” denote the SDSS cutoff $k_{max} = 0.1 h\text{Mpc}^{-1}$, and $0.5 h\text{Mpc}^{-1}$ respectively.

the CMB angular power spectrum C_{Tl} are due to acoustic oscillations in the baryon-photon fluid at the time of last scattering of the CMB photons. As mentioned above, the amplitude of these peaks is determined by Ω_b/Ω_m , while their location is determined by the geometry of the universe, hence there is a near degeneracy in the determination of h , Ω_b , Ω_Λ and Ω_m when only CMB data are considered (Bond et al. 1994; Zaldarriaga, Spergel & Seljak 1997; Huey & Dave 1997).

The turnover in the matter power spectrum is set by the horizon size at matter-radiation equality (e.g., Peebles 1993). Thus, SDSS will make an accurate measurement of $\Omega_m h$. The Silk damping scale, and the acoustic oscillations also affect the transfer function, so that $\Omega_b h$ can also be determined from the SDSS observations (Goldberg & Strauss 1998). Thus combining the MAP and SDSS data allows us to do two important things. First, to the extent that parameters derived from the two independent datasets are consistent, we obtain a powerful check of the correctness of the physical model which ties the two together: gravitational instability theory, the assumption that the fluctuations are adiabatic, and the linear biasing paradigm. This is illustrated in Figure 1, which shows the 68.3% and 95.4% confidence contours in the Ω_b - h (a) and Ω_m - h (b) planes. the dotted lines are for MAP (no polarization) only, the dashed lines are for SDSS only ($k_{max} = 0.5 h\text{Mpc}^{-1}$), and the solid lines are for MAP combined with SDSS. The SCDM model is assumed. Second, the joint analysis of the two independent datasets breaks some of the degeneracies inherent in the MAP data taken alone and improves the accuracy in the determination of parameters.

Table 3: Fisher Matrix $1-\sigma$ error bars for the cosmological parameters of Λ CDM.

1- σ error	MAP ^T	MAP ^T + SDSS ¹	MAP ^T + SDSS ²	MAP ^(T+P)	MAP ^(T+P) + SDSS ¹	MAP ^(T+P) + SDSS ²
$\Delta \ln C_2$	0.10	9.59×10^{-2}	1.20×10^{-2}	4.03×10^{-2}	3.98×10^{-2}	1.18×10^{-2}
$\Delta \ln h$	1.44×10^{-2}	1.43×10^{-2}	1.27×10^{-2}	1.37×10^{-2}	1.36×10^{-2}	1.21×10^{-2}
$\Delta \ln \Omega_\Lambda$	1.44×10^{-2}	1.43×10^{-2}	1.31×10^{-2}	1.39×10^{-2}	1.38×10^{-2}	1.26×10^{-2}
$\Delta \ln(\Omega_b h^2)$	1.69×10^{-2}	1.68×10^{-2}	1.30×10^{-2}	1.56×10^{-2}	1.56×10^{-2}	1.28×10^{-2}
$\Delta \ln \tau_{ri}$	0.61	0.57	9.83×10^{-2}	0.17	0.17	8.58×10^{-2}
$\Delta \ln n_S$	8.98×10^{-3}	8.86×10^{-3}	5.60×10^{-3}	7.11×10^{-3}	7.08×10^{-3}	5.30×10^{-3}
$\Delta \ln b_{eff}$		4.97×10^{-2}	2.34×10^{-2}		3.62×10^{-2}	2.24×10^{-2}

Table 4: Fisher Matrix $1-\sigma$ error bars for the cosmological parameters of O Λ CDM.

1- σ error	MAP ^T	MAP ^T + SDSS ¹	MAP ^T + SDSS ²	MAP ^(T+P)	MAP ^(T+P) + SDSS ¹	MAP ^(T+P) + SDSS ²
$\Delta \ln C_2$	0.14	0.12	1.61×10^{-2}	5.34×10^{-2}	5.23×10^{-2}	1.61×10^{-2}
$\Delta \ln h$	8.26×10^{-2}	7.96×10^{-2}	3.77×10^{-2}	2.44×10^{-2}	2.38×10^{-2}	6.31×10^{-3}
$\Delta \ln \Omega_m$	0.14	0.14	5.66×10^{-2}	2.10×10^{-2}	2.05×10^{-2}	7.48×10^{-3}
$\Delta \ln \Omega_\Lambda$	6.73×10^{-2}	6.23×10^{-2}	2.56×10^{-2}	3.54×10^{-3}	3.53×10^{-3}	3.29×10^{-3}
$\Delta \ln(\Omega_b h^2)$	3.98×10^{-2}	3.80×10^{-2}	2.07×10^{-2}	1.83×10^{-2}	1.80×10^{-2}	1.17×10^{-2}
$\Delta \ln \tau_{ri}$	1.09	1.01	0.33	2.50×10^{-2}	2.47×10^{-2}	1.61×10^{-2}
$\Delta \ln n_S$	2.42×10^{-2}	2.28×10^{-2}	1.13×10^{-2}	8.12×10^{-3}	7.99×10^{-3}	3.84×10^{-3}
$\Delta \ln b_{eff}$		8.44×10^{-2}	2.54×10^{-2}		4.43×10^{-2}	2.45×10^{-2}

Tables 4 and 5 show that the combined data leads to significant improvement on the determination of Ω_m and Ω_Λ compared to considering MAP data alone. Figure 2 shows the 68.3% and 95.4% confidence contours in the Ω_Λ - Ω_m plane in the OCDM model, with the same line types as in Figure 1.

The CMB temperature spectrum is also approximately degenerate in its dependence on the reionization optical depth τ_{ri} and the CMB normalization C_2 , because reionization suppresses the spectrum by a factor of $\exp(-2\tau_{ri})$ on small scales relative to the large scales. Figure 3 shows the confidence contours in the τ_{ri} - C_2 plane. The dotted lines are for MAP (no polarization) only, while the solid lines are for MAP combined with SDSS ($k_{max} = 0.5 \text{ hMpc}^{-1}$). Combining MAP data with SDSS data dramatically breaks the degeneracy between τ_{ri} and C_2 by adding information on the small scales.

Table 5: Fisher Matrix $1-\sigma$ error bars for the cosmological parameters of OCDM.

1- σ error	MAP ^T	MAP ^T + SDSS ¹	MAP ^T + SDSS ²	MAP ^(T+P)	MAP ^(T+P) + SDSS ¹	MAP ^(T+P) + SDSS ²
$\Delta \ln C_2$	0.14	0.11	3.91×10^{-2}	0.11	9.39×10^{-2}	3.73×10^{-2}
$\Delta \ln h$	8.70×10^{-2}	7.86×10^{-2}	3.90×10^{-2}	8.20×10^{-2}	7.61×10^{-2}	3.51×10^{-2}
$\Delta \ln \Omega_m$	0.15	0.12	5.76×10^{-2}	0.14	0.12	5.51×10^{-2}
$\Delta \Omega_\Lambda$	0.11	8.58×10^{-2}	4.01×10^{-2}	0.10	8.31×10^{-2}	3.95×10^{-2}
$\Delta \ln(\Omega_b h^2)$	3.51×10^{-2}	3.13×10^{-2}	1.71×10^{-2}	3.21×10^{-2}	2.88×10^{-2}	1.69×10^{-2}
$\Delta \ln \tau_{ri}$	0.80	0.72	0.52	0.49	0.47	0.39
$\Delta \ln n_S$	1.95×10^{-2}	1.73×10^{-2}	6.83×10^{-3}	1.77×10^{-2}	1.59×10^{-2}	6.75×10^{-3}
$\Delta \ln b_{eff}$			7.57×10^{-2}	3.49×10^{-2}		7.07×10^{-2}
						3.29×10^{-2}

Figures 1-3 show MAP temperature data only, because the extent to which MAP polarization data can be used may be limited by foregrounds (see Section 5). Also, if we allow a cutoff of $k_{max} = 0.5 h \text{ Mpc}^{-1}$ (as we do for the rest of this paper), adding MAP polarization data to the combined MAP and SDSS data does not have a significant impact on the accuracy of the determination of cosmological parameters (see Tables 2-5).

Note that the errors of the parameters from combined MAP and SDSS data are very sensitive to the SDSS cutoff k_{max} . This is as expected, since the small scale information from the SDSS is determined by its cutoff k_{max} . Indeed, in most cases, the galaxy data to $k_{max} = 0.1 h \text{Mpc}^{-1}$ gives only a weak improvement to the constraints the MAP data alone give; much of the improvement comes from the non-linear galaxy regime.

To summarize, when MAP temperature data is considered alone, there is strong degeneracy between the overall amplitude of the matter power spectrum C_2 and the reionization optical depth τ_{ri} , and between the matter density fraction Ω_m and the density fraction contribution from cosmological constant Ω_Λ . Combining MAP and SDSS data dramatically breaks the degeneracy between C_2 and τ_{ri} , and reduces the degeneracy between Ω_m and Ω_Λ , leading to a significant improvement on the determination of C_2 , τ_{ri} , Ω_m , and Ω_Λ , enabling us to measure the effective bias between the matter power spectrum and the galaxy redshift power spectrum b_{eff} . The accuracy in the determination of other cosmological parameters is also improved by combining MAP and SDSS data, but to a less impressive extent. In the next section, we study the model-independent measurement of the primordial power spectrum, which can only be achieved by using the combined MAP and SDSS data.

4. Measurement of the Primordial Power Spectrum

We now consider a more general primordial power spectrum. We parameterize the primordial power spectrum $A_S^2(k)$ as

$$A_S^2(k) = \begin{cases} a_1, & \text{for } k < k_1, \\ a_i, & \text{for } k_{i-1} < k < k_i, \quad i > 1 \end{cases} \quad (20)$$

where $k_1 = 0.001 h\text{Mpc}^{-1}$, and k_i ($i = 2, 3, \dots, 20$) are equally spaced in $\log k$ from k_1 to $k = 0.5h\text{Mpc}^{-1}$. The a_i ($i = 1, 2, \dots, 20$) are taken to be independent variables. The derivative of the C_l 's with respect to a_i are taken to be finite differences with stepsize of 5% the model value of a_i . The derivative of the galaxy power spectrum with respect to a_i are given by

$$\frac{\partial \ln P_G(k)}{\partial a_i} = \begin{cases} \frac{\partial \ln f_{NL}(x)}{\partial \ln x} \frac{1}{a_i}, & \text{for } k < k_1 \text{ (}i = 1\text{), or } k_{i-1} < k < k_i \text{ (}i > 1\text{),} \\ 0, & \text{otherwise,} \end{cases} \quad (21)$$

where x and $f_{NL}(x)$ are the same as in Equation (19). We assume that the cosmological parameters are known to be that of the SCDM model (with $A_S^2(k) = 1$) listed in Table 1.

In this section, we take the cutoff wavenumber of the SDSS to be $k = 0.5\text{Mpc}^{-1}$ throughout, and we consider the MAP temperature data only in this section; adding the polarization data does not have a significant effect on errors from the combined MAP and SDSS data.

Figure 4 shows the accuracy in the determination of the bin amplitudes of the primordial power spectrum, $k A_S^2(k)$; the $1-\sigma$ error bars are shown for MAP only (a), SDSS only (b), and MAP and SDSS combined (c). (Note that in Figure 4(b), the error bars which extend out of the box on both ends are infinities, because the SDSS has a characteristic survey length R ; it can not measure modes smaller than $k_{min} = 2\pi/R$, and the modes which are approximately statistically independent are separated by k_{min} .) Assuming the cosmological parameters are known, for 20 bins in $\log k$ ($k \leq 0.5h\text{Mpc}^{-1}$), the primordial power spectrum can be determined to around 10% accuracy for $k \sim 0.01\text{Mpc}^{-1}$, and to around 1% accuracy for $k \sim 0.1\text{Mpc}^{-1}$ (see Figure 4(c)) by combining MAP and SDSS data.

Not surprisingly, the determination of the primordial power spectrum bin amplitudes does depend on the assumed knowledge of the cosmological parameters. Figure 5(a) shows the effect of including four cosmological parameters (h , Ω_Λ , Ω_b , and τ_{ri}) in the parameter estimation for MAP data only. The error bars on the primordial power spectrum bin amplitudes are dramatically larger in Figure 5(a) than in Figure 4(a).

Figure 5(b) shows the effect of including the SDSS data in the analysis, adding the galaxy bias b_{eff} as a fifth parameter. The uncertainty in the determination of the primordial power spectrum bin amplitudes a_i increases by a factor of less than 2 relative to the case

in which the cosmological parameters are known *a priori* (Figure 4(c)). This difference is indistinguishable in the figures, because the error bars are only of the order of 1%. Comparison of Figure 5(a) and Figure 5(b) illustrates the critical importance of combining the MAP data with the SDSS data in the determination of the primordial power spectrum bin amplitudes.

Note that our choice of 20 bins in $\log k$ to parameterize $A_S^2(k)$ is somewhat arbitrary. Obviously, the errors on the bin amplitudes would increase if we were to increase the number of bins. When the cosmological parameters are estimated together with the $A_S^2(k)$ bin amplitudes a_i , we expect the covariance between the cosmological parameters and the a_i 's to increase rapidly with smaller bin size, as the primordial power spectrum becomes flexible enough to mimic the Doppler peaks and other features of the C_l .

To illustrate how the errors on the cosmological parameters change as they are estimated jointly with primordial power spectrum bin amplitudes, we show in Table 6 the Fisher matrix 1- σ error bars for two groups of cosmological parameters, $(h, \Omega_b, \tau_{ri}, b_{eff})$ and $(h, \Omega_\Lambda, \Omega_b, \tau_{ri}, b_{eff})$, when they are estimated jointly within each group and when each group is simultaneously estimated with 20 independent bin amplitudes of the primordial power spectrum. The cosmological parameters can still be determined to impressive

Table 6: Fisher Matrix 1- σ error bars for the cosmological parameters.

1- σ error	4 parameters	4 parameters & 20 bin amplitudes of $A_S^2(k)$	5 parameters	5 parameters & 20 bin amplitudes of $A_S^2(k)$
$\Delta \ln h$	5.22×10^{-3}	6.82×10^{-3}	1.76×10^{-2}	2.29×10^{-2}
$\Delta \Omega_\Lambda$			4.26×10^{-2}	5.41×10^{-2}
$\Delta \ln(\Omega_b h^2)$	1.59×10^{-2}	3.91×10^{-2}	1.61×10^{-2}	4.43×10^{-2}
$\Delta \ln \tau_{ri}$	5.63×10^{-2}	0.20	0.11	0.24
$\Delta \ln b_{eff}$	5.53×10^{-3}	9.43×10^{-3}	1.31×10^{-2}	1.73×10^{-2}

accuracy even when they are estimated simultaneously with 20 independent bin amplitudes of the primordial power spectrum! Of course, we do not include the overall amplitude of the power spectrum C_2 as a free parameter, as it is degenerate with the a_i by definition.

Figures 4 and 5 assume that the true primordial power spectrum is $A_S^2(k) = 1$. For the purpose of illustration, we can choose our model primordial power spectrum $A_S^2(k)$ to have broken scale-invariance based on the Holman et al. (1991) and Adams et al. (1997) models. We write

$$A_S^2(k) = \begin{cases} 1, & k < 0.01 \text{ hMpc}^{-1}, \\ A + B k, & 0.01 \text{ hMpc}^{-1} < k < 0.1 \text{ hMpc}^{-1}, \\ 0.25 k^{-0.2}, & k > 0.1 \text{ hMpc}^{-1}, \end{cases} \quad (22)$$

where A and B are chosen such that $A_S^2(k)$ is continuous. Figure 6 shows the primordial power spectrum of Equation (22) with $1-\sigma$ error bars for the combined MAP and SDSS data. Clearly, the accuracy in the determination of $A_S^2(k)$ is not sensitive to the assumed underlying model; the errors on $A_S^2(k)$ bin amplitudes do not change significantly with model where the errors are larger than of order 1%.

There have been recent claims of possible observational detection of features in the matter power spectrum on the scale of $k \sim 0.1 h\text{Mpc}^{-1}$ (Peacock 1997). Combining MAP and SDSS data will enable us to confirm such features, and determine in a model-independent way whether they are intrinsic to the primordial power spectrum. It would be straightforward to translate our bin amplitude errors of the primordial power spectrum into constraints on existing inflationary models; our errors are small enough to be very interesting. However, it is perhaps more exciting to anticipate that the model-independent measurement of the primordial power spectrum in wavenumber bins from the combined MAP and SDSS data will provide a lead to the correct inflationary model.

5. Summary

Cosmic microwave background experiments measure fluctuations in the curvature of space at the surface of last scattering. If the primordial fluctuations are adiabatic, then MAP will be a sensitive probe of the geometry of the universe, the matter/photon ratio ($\Omega_m h^2$), the baryon/photon ratio ($\Omega_b h^2$) and the primordial power spectrum for $k < 0.2 h\text{Mpc}^{-1}$.

Observations of large scale structure measure the large scale distribution of galaxies. If the primordial fluctuations are adiabatic, then SDSS will be a sensitive probe of the primordial power spectrum for $k > 0.02 h\text{Mpc}^{-1}$ and $\Omega_m h$, which determines the horizon size at matter-radiation equality and thus the shape of the processed power spectrum. SDSS will also be a powerful probe of the nature of the dark matter (Hu et al. 1997).

The combination of the SDSS and the MAP data will be a powerful test of our basic cosmological models. Both experiments will accurately determine the amplitude of density fluctuations at $0.2 > k > 0.02 h\text{Mpc}^{-1}$. Will there be a set of cosmological parameters and primordial power spectrum that is consistent with both sets of observations? If so, then we will have tested the gravitational structure formation paradigm, our interpretation of the primordial fluctuations as adiabatic, and the linear biasing paradigm. If not, this conflict will likely lead us to a deeper understanding of the origin of structure in the universe.

In particular, from the combination of the MAP and SDSS data, we can obtain a model-independent measurement of the primordial power spectrum, assuming that the primordial fluctuations are adiabatic. If the values of the cosmological parameters that best fit the data are close to what we expect, but the primordial power spectrum differs

significantly from the predictions of the current inflationary models, then it will be an indication of new physics in the early universe, and it will provide a solid starting point for building new inflationary models.

If there is a theory consistent with both data sets, then the combination of the two observations will break the degeneracies inherent in each individual observation. Cosmic microwave background observations by themselves measure a combination of the amplitude of the primordial power spectrum and the optical depth. Large scale structure observations measure the product of the current matter power spectrum and the bias parameter. In linear theory, the offset between the power spectrum as determined by the two sets of observations determines a combination of the bias parameter and the optical depth of the universe. Because of non-linear effects on the spectrum, this offset is scale-dependent, this will enable us to independently measure the bias parameter and the optical depth of the universe. The combination of the two experiments will also improve our ability to determine other cosmological parameters, in particular, the matter density and the cosmological constant.

Measurements of the cosmic microwave background polarization can provide an independent measure of the optical depth of the universe τ_{ri} (Zaldarriaga, Spergel & Seljak 1997). However, emission from both polarized galactic dust and synchrotron emission (Keating et al. 1997) may swamp the primordial polarization fluctuations at large angular scales. These foregrounds may significantly limit our ability to extract useful cosmological information from polarization measurements. Hence it is important that we can use the SDSS data as an alternative and independent aid to MAP in the determination of τ_{ri} .

The Sloan Digital Survey, and other large scale structure surveys, will make other independent measurements that will probe cosmological parameters and the primordial spectrum: redshift distortions, cluster properties, small scale velocity fields, and the evolution of structure. These will provide additional tests of the basic model and will further enhance our ability to measure cosmological parameters.

With this in mind, there are a number of improvements that could be done in this analysis. The redshift distortions could be measured directly, and the effects could be included directly into the Fisher matrix analysis (cf., de Laix & Starkman 1997 and Hatton & Cole 1997 for a discussion of how well redshift-space distortions can be measured from the SDSS data). Similarly, we could parameterize the effects of galaxy and clustering evolution, and include these as parameters in the analysis. More challenging will be a proper accounting of non-linear effects on small scales. The analyses in Tables 2-5 show that going to $k_{max} = 0.5 \text{ } h\text{Mpc}^{-1}$ gives us particularly strong constraints on cosmological parameters, but we have taken the non-linear effects into account in only a relatively crude way in this paper.

The next few years will be a very exciting time in cosmology.

6. Acknowledgements

Y.W. acknowledges partial support from NSF grant AST94-19400. DNS acknowledges support from the MAP/MIDEX project. MAS acknowledges support from the Alfred P. Sloan Foundation, a fellowship from Research Corporation, and NSF grant AST96-16901. We acknowledge the use of CMBFAST Boltzmann code by Uroš Seljak and Matias Zaldarriaga. It is a pleasure for us to thank Matias Zaldarriaga for many helpful clarifications concerning CMBFAST.

REFERENCES

- Adams, J.A., Ross, G.G., & Sarkar, S. 1997, preprint (hep-ph/9704286)
- Allen, B., & Koranda, S. 1995, Phys. Rev. D52, 1902
- Bennett, C.L., Halpern, M., Hinshaw, G., Jarosik, N., Limon, M., Mather, J., Meyer, S.S., Page, L., Spergel, D.N., Tucker, G., Wilkinson, D.T., Wollack, E. & Wright, E.L. 1997, BAAS, 29, 1353
- Bond, J. R., Crittenden, R., Davis, R.L., Efstathiou, G., & Steinhardt, P.J. 1994, Phys. Rev. Lett., 72, 13
- Bond, J.R., Efstathiou, G., & Tegmark, M. 1997, MNRAS, 291, L33
- Bunn, E.F. & White, M. 1997, ApJ, 480, 6
- Carroll, S.M., Press, W.H., & Turner, E.L. 1992, ARA&A, 30, 499
- Cole, S., Hatton, S., Weinberg, D.H., & Frenk, C.S. 1998, preprint (astro-ph/9801250)
- Copeland, E.J., Grivell, I.J., & Liddle, A.R. 1997, preprint (astro-ph/9712028)
- Crittenden, R., Bond, J.R., Davis, R.L., Efstathiou, G., & Steinhardt, P.J. 1993, Phys. Rev. Lett. 71, 324
- de Laix, A.A., & Starkman, G. 1997, ApJ, in press (astro-ph/9707008)
- Dodelson, S., Hui, L., & Jaffe, A. 1997, preprint (astro-ph/9712074)
- Dodelson, S., Kinney, W.H., & Kolb, E.W. 1997, Phys. Rev. D, 56, 3207
- Dodelson, S., Knox, L., & Kolb, E.W. 1994, Phys. Rev. Lett. 72, 3444
- Eisenstein, D.J. & Hu, W. 1997, astro-ph/9709112
- Feldman, H.A., Kaiser, N., & Peacock, J.A. 1994, ApJ, 426, 23
- Fisher, K.B., & Nusser, A. 1996, MNRAS, 279, L1
- Freese, K., Frieman, J.A., & Olinto, A.V. 1990, Phys. Rev. Lett., 65, 3233
- Fry, J.N., & Wang, Y. 1992, Phys. Rev., D46, 3318
- Gelfand, I.M., Minlos, R.A., & Shapiro, Z. Ya. 1963, Representations of the Rotation and Lorentz Groups and Their Applications (Pergamon:Oxford)
- Goldberg, J.N., et al. 1967, J. Math. Phys., 8, 2155

- Goldberg, D.M., & Strauss, M.A. 1998, ApJ, 495, in press
- Gunn, J. E., & Weinberg, D. H. 1995, in *Wide-Field Spectroscopy and the Distant Universe*, ed. S. J. Maddox and A. Aragón-Salamanca (Singapore: World Scientific), 3
- Hamilton, A.J.S. 1997, preprint (astro-ph/9708102)
- Hatton, S.J., & Cole, S. 1997, MNRAS, in press (astro-ph/9707186)
- Holman, R., Kolb, E.W., Vadas, S.L., & Wang, Y. 1991a, Phys. Rev., D43, 3833
- Holman, R., Kolb, E.W., Vadas, S.L., & Wang, Y. 1991b, Phys. Lett., B269, 252
- Hu, W., Eisenstein, D.J., & Tegmark, M. 1997, preprint (astro-ph/9712057)
- Huey, G. & Dave, R. 1997, University of Pennsylvania preprint UPR-767T
- Jain, B., & Bertschinger, E. 1994, ApJ, 431, 495
- Jungman, G., Kamionkowski, M., Kosowsky, A., & Spergel, D.N. 1996, Phys. Rev., D54, 1332
- Kaiser, N. 1987, MNRAS, 227, 1
- Kofman, L., & Linde, A. 1987, Nucl Phys B282, 555
- Kamionkowski, M., Kosowsky, A., & Stebbins, A. 1997, Phys. Rev. Lett., 78, 2058
- Kauffmann, G., Nusser, A., & Steinmetz, M. 1997, MNRAS, 286, 795
- Keating, B., Timbie, P., Polnarev, A. & Steinberger, J. 1997, ApJ, in press (astro-ph/9710087)
- Kendall, M.G. & Stuart, A. 1969, *The Advanced Theory of Statistics, Volume II*, Griffin, London
- Kolb, E.W. 1996, in *Proceedings of Erice School, Astrofundamental Physics*, astro-ph/9612138
- Kolb, E.W., & Turner, M.S. 1990, *The Early Universe* (Addison-Wesley Publishing Company)
- La, D., & Steinhardt, P.J. 1991, Phys. Rev. Lett., 62, 376
- Lesgourgues, J., Polarski, D., & Starobinsky, A.A. 1997, preprint (astro-ph/9711139)
- Lidsey, J.E., Liddle, A.R., Kolb, E.W., Copeland, E.J., Barriero, T. & Abney, M. 1997, Rev. Mod. Physics, 69, 373

- Linde, A.D. 1983, Phys. Lett., 129B, 177
- Lineweaver, C. & Barbosa, D. 1998, A&A 329, 799
- Peacock, J.A. 1997, MNRAS, 284, 885
- Peacock, J.A., & Dodds, S.J. 1996, MNRAS, 280, L19
- Peebles, P.J.E. 1993, *Principles of Physical Cosmology* (Princeton: Princeton University Press)
- Scherrer, R.J., & Weinberg, D.H. 1997, preprint (astro-ph/9712192)
- Seljak, U. 1996, ApJ, 482, 6
- Seljak, U., & Zaldarriaga, M. 1996, ApJ, 469, 437
- Spergel, D.N. 1994, BAAS, 26, 1427
- Strauss, M.A. 1997, in *Formation of Structure in the Universe*, edited by Avishai Dekel and Jeremiah P. Ostriker (Cambridge: Cambridge University Press), in press
- Tegmark, M. 1997, Phys. Rev. Lett., 79, 3806
- Tegmark, M., Hamilton, A.J.S., Strauss, M.A., Vogeley, M.S., & Szalay, A.S. 1998, ApJ, 499, in press (astro-ph/9708020)
- Tegmark, M., Taylor, A. & Heavens, A. F. 1997, ApJ, 480, 22
- Turner, M.S. 1997, preprint (astro-ph/9704062)
- Turner, M.S., & Wang, Y. 1996, Phys. Rev., D53, 5727
- Wang, Y. 1994, Phys. Rev., D50, 6135
- Wang, Y. 1996, Phys. Rev., D53, 639
- Webster, M., Hobson, M.P., Lasenby, A.N., Laha, O., & Rocha, G. 1998, preprint (astro-ph/9802109)
- Weinberg, D. H. 1995, in *Wide-Field Spectroscopy and the Distant Universe*, eds. S. J. Maddox and A. Aragón-Salamanca (Singapore: World Scientific), 129
- Zaldarriaga, M., & Seljak, U. 1997, Phys. Rev., D55, 1830
- Zaldarriaga, M., Spergel, D.N., & Seljak, U. 1997, ApJ, 488, 1

Fig. 1.— The confidence contours (68.3% and 95.4%) in the Ω_b - h (a) and Ω_m - h (b) planes for the SCDM model. The dotted lines are for MAP (no polarization) only, the dashed lines are for SDSS to $k_{max} = 0.5 \text{ hMpc}^{-1}$ only, and the solid lines are for MAP combined with SDSS.

Fig. 2.— The confidence contours (68.3% and 95.4%) in the Ω_Λ - Ω_m plane for the OCDM model. The line types are the same as in Figure 1.

Fig. 3.— The confidence contours (68.3% and 95.4%) in the τ_{ri} - C_2 plane for the SCDM model. The dotted lines are for MAP (no polarization) only, the solid lines are for MAP combined with SDSS.

Fig. 4.— The primordial power spectrum with $1-\sigma$ error bars for MAP only (a), SDSS only (b), and MAP and SDSS combined (c), assuming that the cosmological parameters are known to be that of the SCDM model (with $A_S^2(k) = 1$) listed in Table 1.

Fig. 5.— The primordial power spectrum with $1-\sigma$ error bars. (a) MAP data only, with four cosmological parameters ($h, \Omega_\Lambda, \Omega_b, \tau_{ri}$) included in the parameter estimation; (b) Combined data of MAP and SDSS, with five cosmological parameters ($h, \Omega_\Lambda, \Omega_b, \tau_{ri}, b$) included in the parameter estimation.

Fig. 6.— The primordial power spectrum of Equation (22) with $1-\sigma$ error bars for the combined MAP and SDSS data.

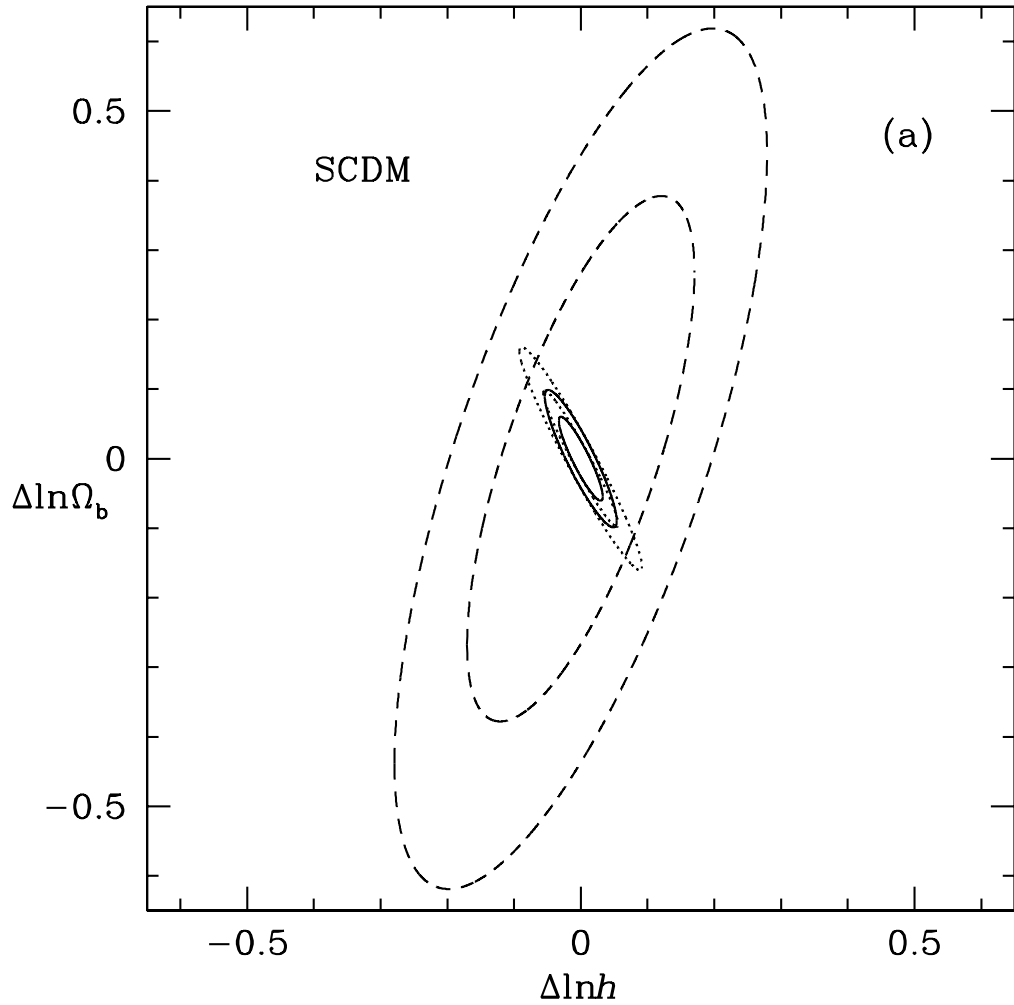


Fig. 1.— (a) The confidence contours (68.3% and 95.4%) in the Ω_b - h planes assuming the SCDM model. The dotted lines are for MAP (no polarization) only, the dashed lines are for SDSS to $k_{max} = 0.5 h\text{Mpc}^{-1}$ only, and the solid lines are for MAP combined with SDSS.

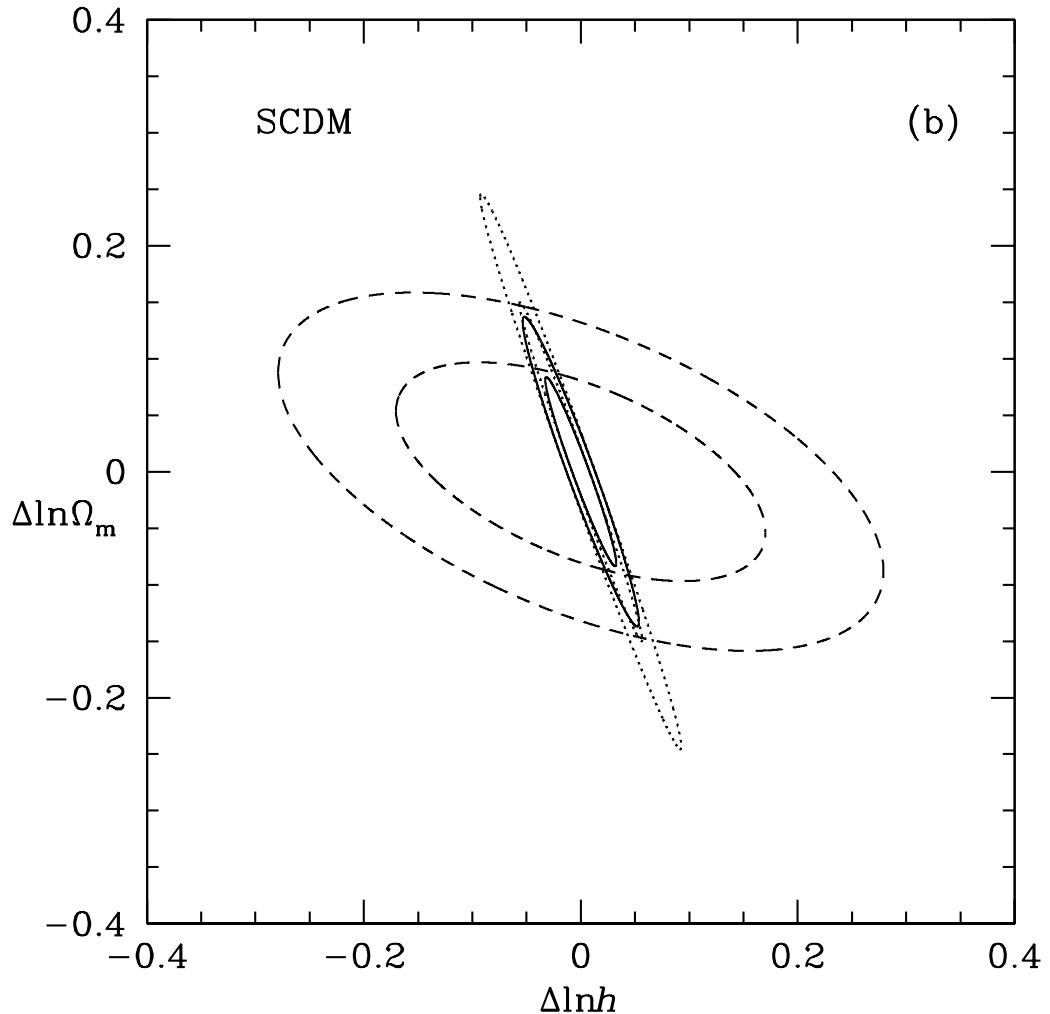


Fig. 1.— (b) The confidence contours (68.3% and 95.4%) in the Ω_m - h planes. The dotted lines are for MAP (no polarization) only, the dashed lines are for SDSS only, the solid lines are for MAP combined with SDSS.

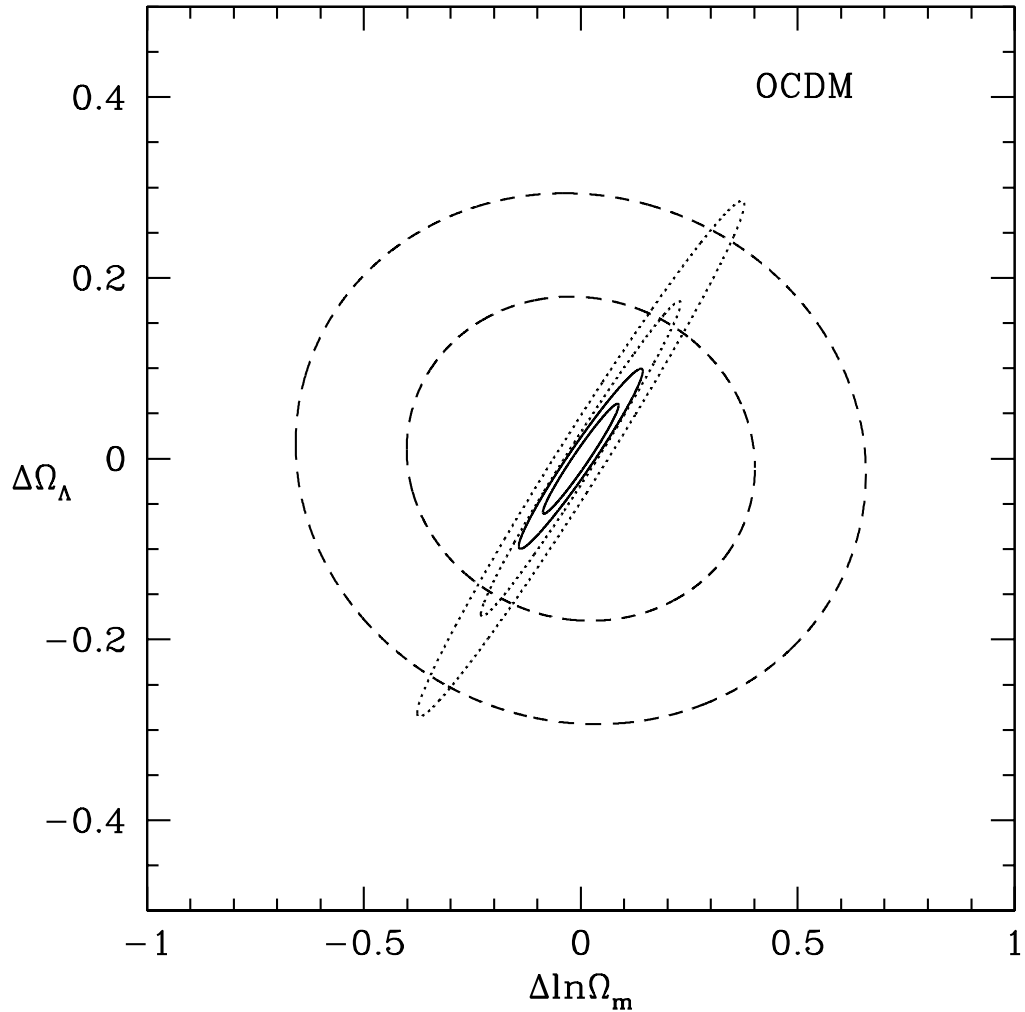


Fig. 2.— The confidence contours (68.3% and 95.4%) in the Ω_Λ - Ω_m plane for the OCDM model. The line types are the same as in Figure 1.

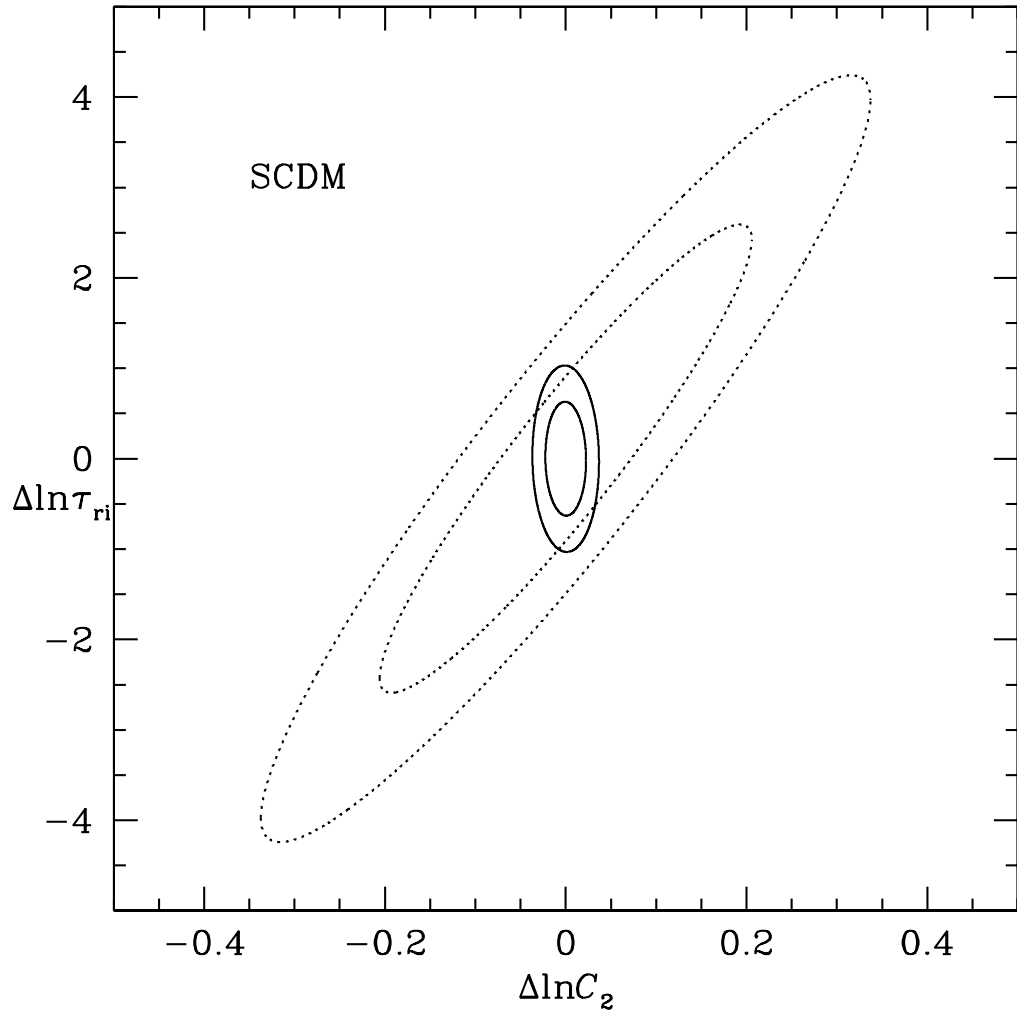


Fig. 3.— The confidence contours (68.3% and 95.4%) in the τ_{ri} - C_2 plane for the SCDM model. The dotted lines are for MAP (no polarization) only, the solid lines are for MAP combined with SDSS.

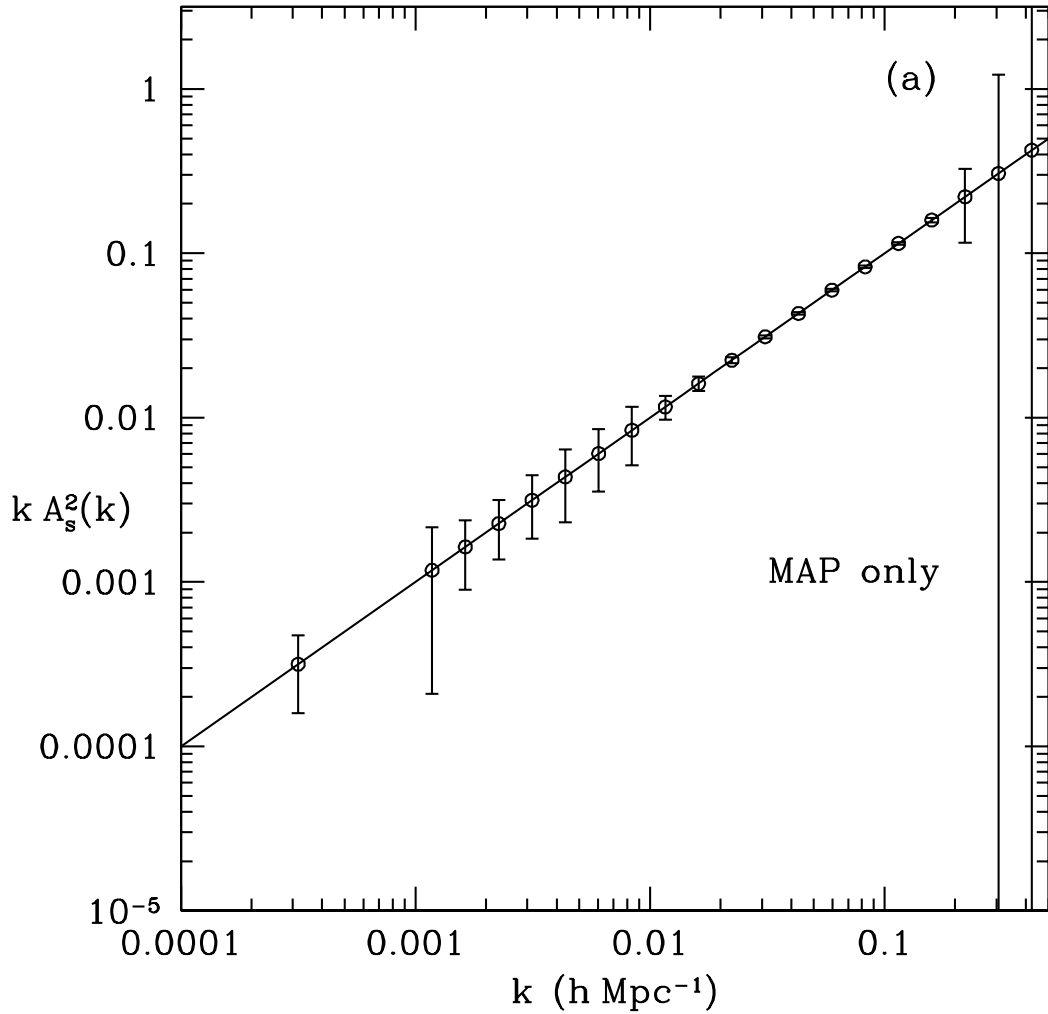


Fig. 4.— The primordial power spectrum with $1-\sigma$ error bars, assuming that the cosmological parameters are known to be that of the SCDM model (with $A_S^2(k) = 1$) listed in Table 1. (a) MAP only.

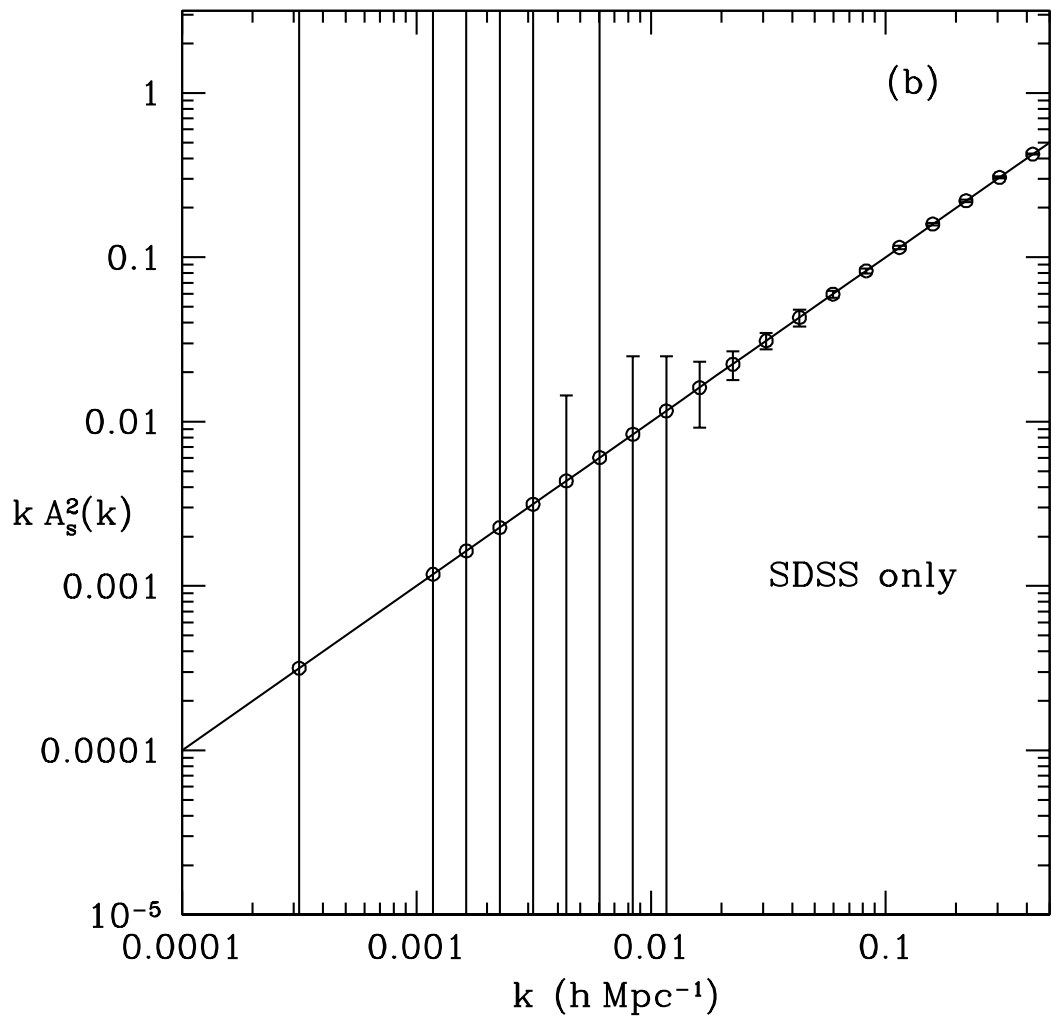


Fig. 4.— (b) SDSS only.

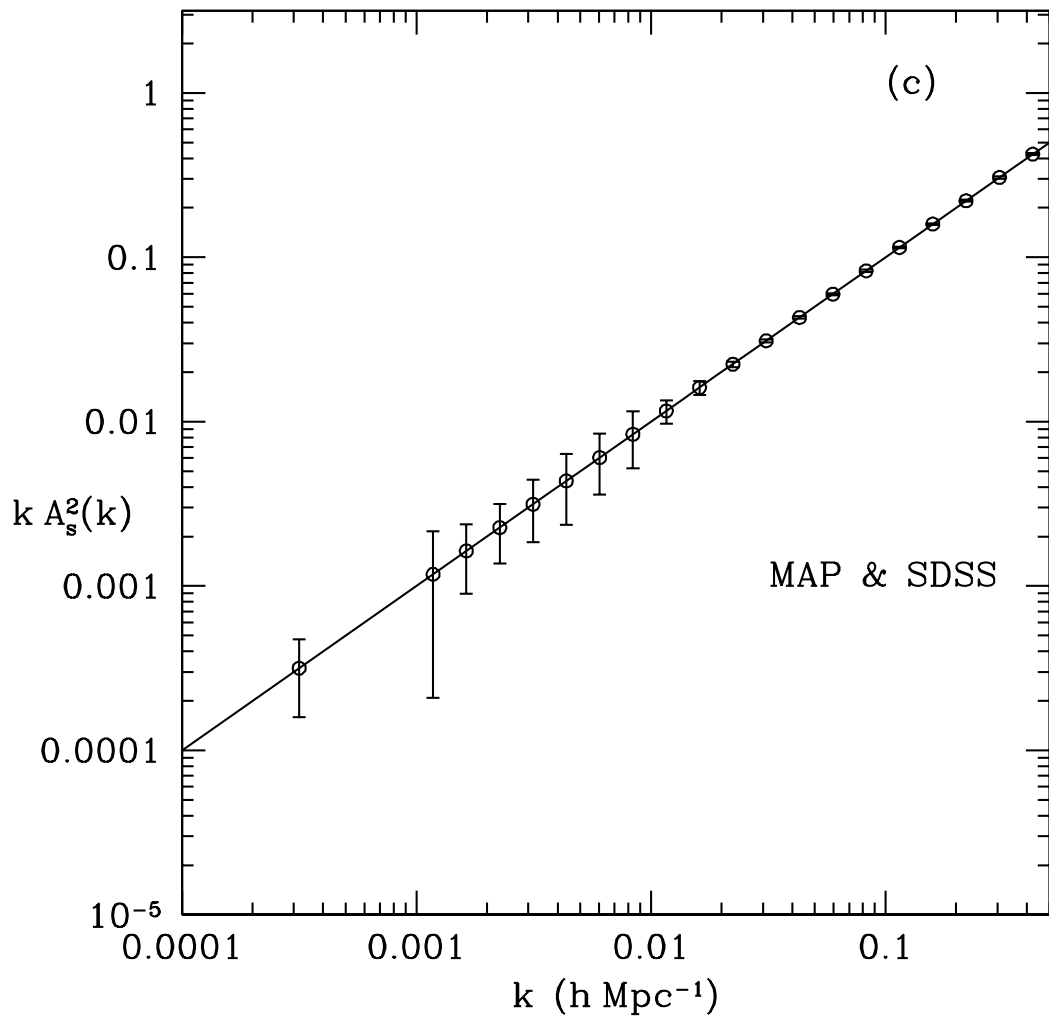


Fig. 4.— (c) MAP and SDSS combined.

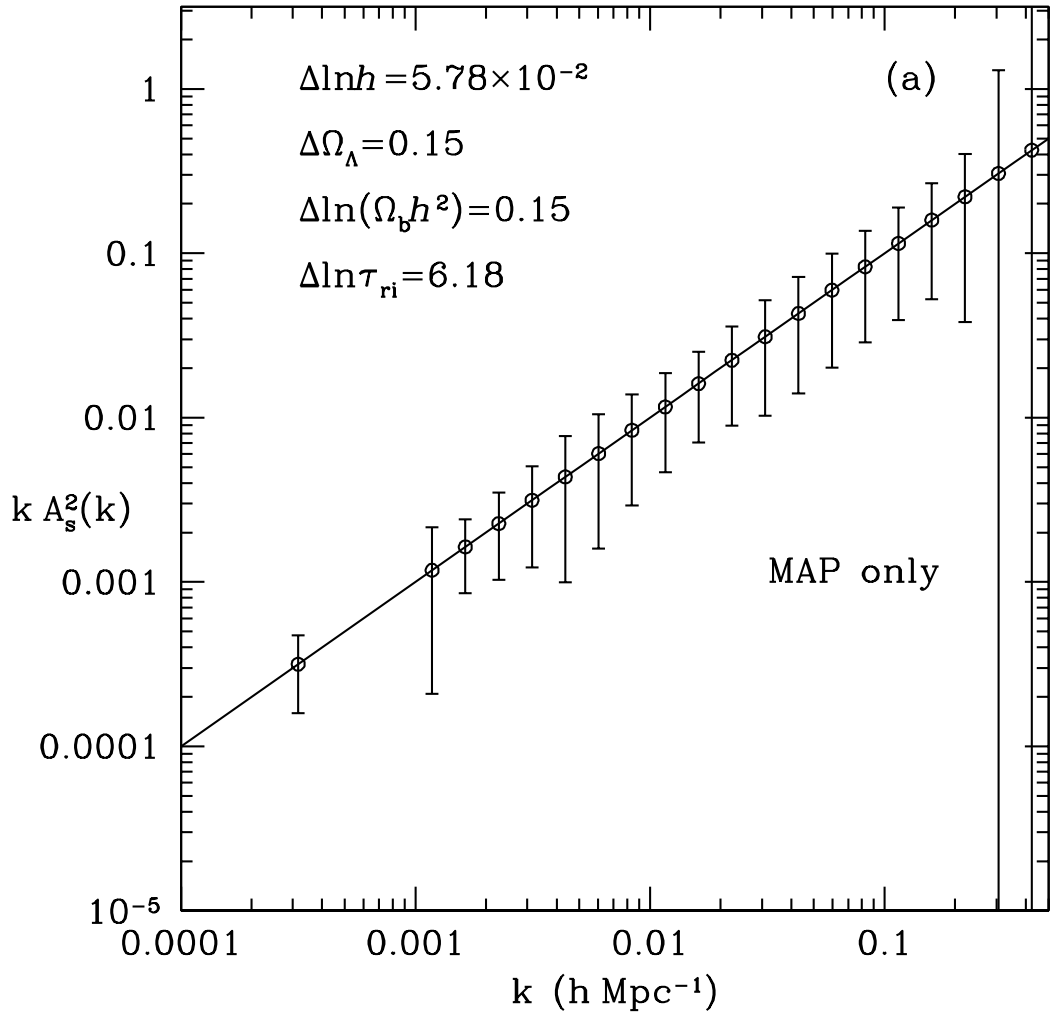


Fig. 5.— The primordial power spectrum with $1-\sigma$ error bars. (a) MAP data only, with four cosmological parameters (h , Ω_Λ , Ω_b , τ_{ri}) included in the parameter estimation.

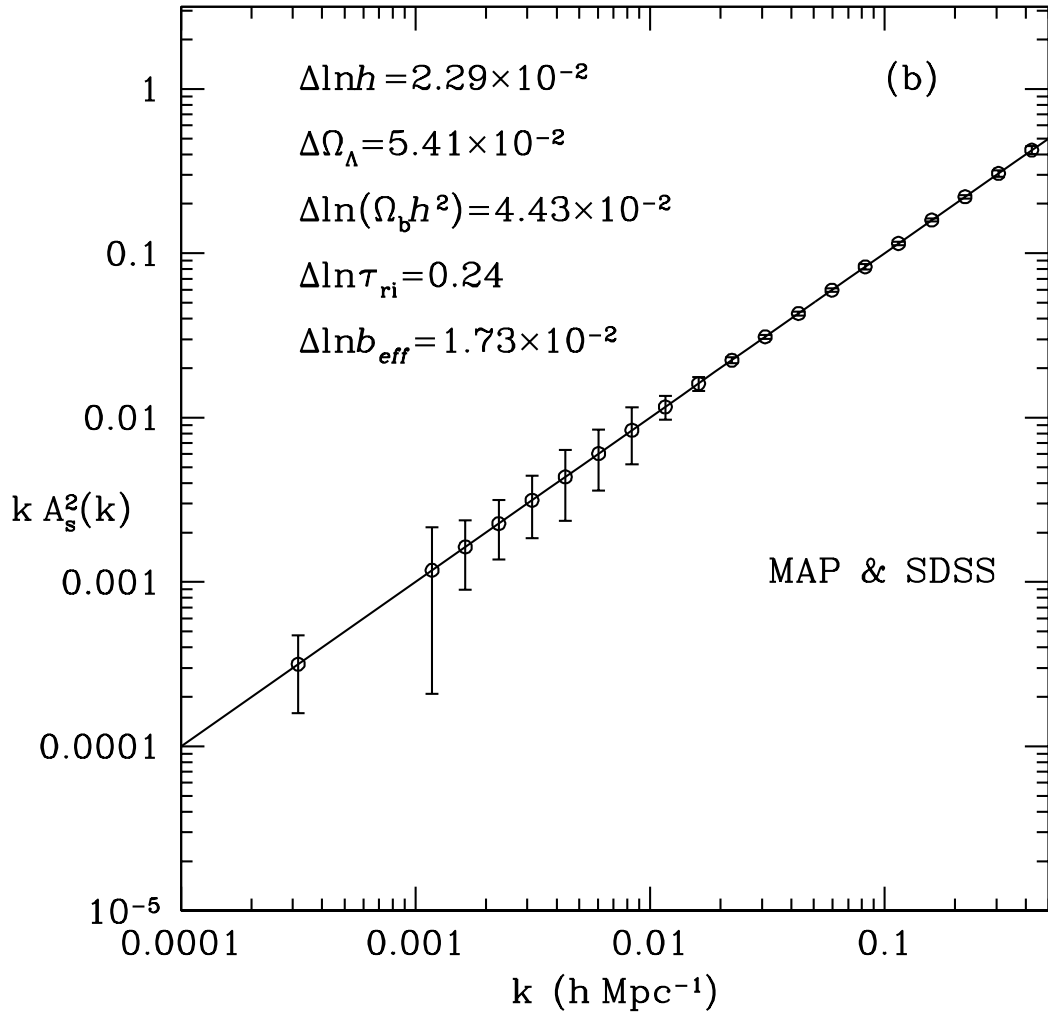


Fig. 5.— (b) Combined data of MAP and SDSS, with five cosmological parameters (h , Ω_Λ , Ω_b , τ_{ri} , b) included in the parameter estimation.

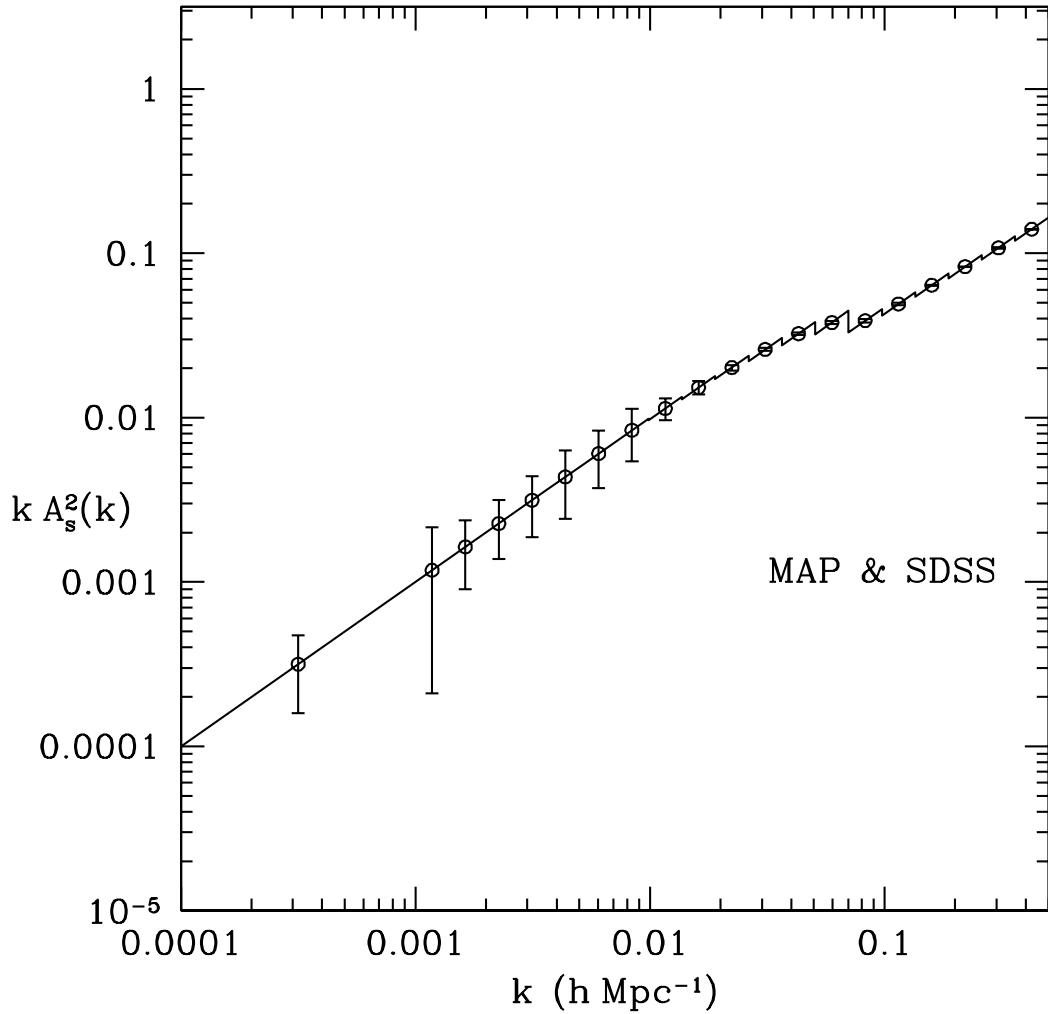


Fig. 6.— The primordial power spectrum of Equation (22) with $1-\sigma$ error bars for the combined MAP and SDSS data.